Journal of Sound and Vibration (2001) **248**(4), 671–694
doi:10.1006/jsvi.2001.3818, available online at http://www.idealibrary.com on IDEAL®

SLIDING FRICTION-INDUCED NON-LINEARITY AND PARAMETRIC EFFECTS IN GEAR DYNAMICS

M. VAISHYA AND R. SINGH

Acoustics and Dynamics Laboratory, Department of Mechanical Engineering, The Ohio State University, Columbus, OH 43210-1107, *U.S.A. Email singh.3@osu.edu*

(*Received* 11 *December* 2000, *and in final form* 10 *May* 2001)

The mechanism of gear meshing entails a large amount of sliding between the mating teeth in contact. Friction forces act orthogonal to the line of action, and the resulting dynamic force and moment are governed by a number of parameters, such as the relative surface speed, instantaneous load and spatial location of the point of contact. Sliding resistance is inherently non-linear in nature, and due to the additional presence of periodic meshing properties like stiffness and viscous damping, dynamic interactions result between friction and system parameters. This combination leads to a non-linear time-varying (NLTV) system comprising implicit non-linear differential equations. Nevertheless, most researchers have treated friction as a linear time-varying (LTV) phenomenon. In this article, both of these models are critically analyzed. For the LTV system, the harmonic balance formulation is developed to predict the dynamic behavior and sub-harmonic instabilities in the system. The NLTV analysis leads to very complex and intractable equations, and hence numerical methods are applied. Using this analysis, the physical phenomena associated with the two models are compared and the essential differences in the system behavior are examined. Finally, the dynamic effects of friction-induced non-linearity are investigated and the critical parameters are identified.

1. INTRODUCTION

During the gear meshing action, the gear and the pinion momentarily undergo a pure rolling action as the zone of contact coincides with the pitch point. In all other positions, however, the meshing action is a combination of rolling and sliding. Since rolling resistance is considerably smaller than the sliding resistance [1, 2], its contribution to the total tooth friction is usually ignored. Unlike the total rolling speed of the gears, the relative sliding velocity varies with the meshing position as well as from one tooth to the other. A mean instantaneous sliding speed for each tooth pair in contact can be derived from meshing kinematics. However, the true value of the sliding velocity will also include a component from the oscillating torsional motion of the gear and pinion. This dependency upon the instantaneous vibratory velocity introduces an implicit non-linearity in the gear dynamic system, which assumes the form of a non-linear time-varying (NLTV) system.

Typically, the operating regime of the gears must be characterized by many simultaneous dynamic phenomena, such as periodically varying meshing stiffness and damping, multiple excitations and sliding resistance between the mating gear teeth in contact. Consequently, gears functioning under sliding friction may exhibit sub-harmonic response, multiple solutions, super-harmonic resonance, modulation and dynamic instabilities. For analysis of friction effects in a gear mesh, some researchers have applied a linear time-varying (LTV)

0022-460X/01/490671 + 24 $35.00/0

model for estimating the coefficient of friction [2–7]. Alternatively, equivalent linear viscous damping has been proposed as a substitution for the energy losses ensuing from friction [4, 8]. Clearly, both these methods have limitations and certain non-linear dynamic phenomena such as sub-harmonic response may not be detected. In the absence of friction, other non-linearities, most notably those due to tooth backlash, have been thoroughly investigated by several authors [8–15]. The problem of friction at the tooth contact is different from classical friction oscillators in that the direction of sliding resistance is not the same as the primary motion direction or degree of freedom. Hence the conventional knowledge of friction oscillators [16] may not be applicable in this study.

In a gear mesh, sliding friction can affect the system dynamics in four distinct ways, namely as an external excitation, as a periodic system parameter, as a non-linear coupling agent and as a source of energy dissipation. In its simplest form, sliding friction can be modelled as an external excitation with the same fundamental period as the gear meshing cycle. This method has been studied extensively by several researchers [2, 3, 5, 6] using different dynamic models. If the sliding mechanism is formulated in a more intricate manner such as based on the dynamic mesh force [2, 7], then the friction term appears on the left-hand side of the equation and thus it participates as a time-varying parameter in the system. Thirdly, due to the dependence of friction on the instantaneous sliding velocity, an implicit non-linearity occurs, which introduces dynamic coupling between system parameters and sliding mechanism [4]. Finally, sliding resistance can influence the system with its damping characteristics, as discussed by Iida *et al.* [4] and Velex and Cahouet [2]. This paper describes a new methodology to examine these issues, using a simplified model of a spur gear pair operating under sliding friction at the tooth interface. In particular, the dynamic model is used to examine the effects of friction non-linearities in the system in the presence of time-varying mesh parameters.

2. SCOPE AND OBJECTIVES

In the current article, the spur gear pair is modelled as a two-d.o.f. torsional system, as shown in Figure 1. The gear teeth deform as a result of Hertzian stress as well as the cantilever bending of the teeth [17], and the corresponding mesh stiffness is represented by $k(t)$. Surface profiles of the teeth exhibit deviations from the perfect involute shape, either due to manufacturing errors or deliberate modifications. This non-conjugacy of the tooth profiles acts as a displacement excitation at the mesh, referred to as the unloaded static transmission error $\varepsilon(t)$. Additionally, external torques T_p and T_g act on the pinion and the gear respectively. The mean angular speeds of the pinion and gear are Ω_p and Ω_g, whereas θ_p and θ_g represent the angular displacement from the mean position. In general, the surface velocities of the gear and pinion are unequal at the tooth interface, resulting in a relative sliding velocity and a friction resistance acting at the contact zone.

For most practical designs of spur gears, the profile contact ratio Γ varies between 1·0 and 2·0. This implies that two teeth are in contact for $(\Gamma - 1)$ fraction of total time, and a single tooth transmits the torque during the rest of the mesh cycle. In this study, the beginning of the mesh cycle at $t = 0$ is defined to be coincident with the initiation of contact for the second tooth. As the gears roll, the first tooth leaves contact and there is a sudden reduction in the meshing stiffness $k(t)$ of the system. At this instant t_a, the load on the second tooth is doubled, since the load is assumed to be distributed equally amongst all the teeth in contact. The second critical point occurs at t_b when the zone of contact passes through the pitch point, and the direction of the sliding velocity for tooth 2 reverses. Note that the order in which t_a and t_b occur is dependent on the specific gear

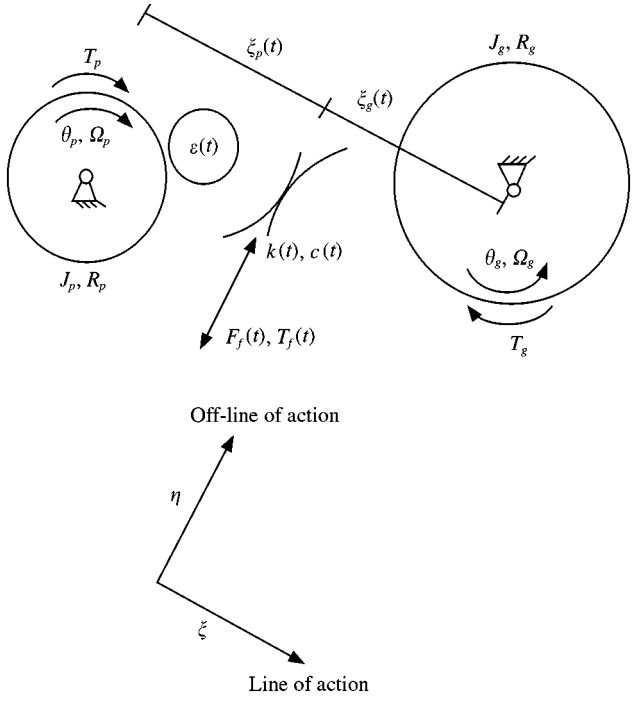

Figure 1. Dynamic model of a gear pair operating with sliding friction.

geometry. Finally, the third gear tooth comes into engagement at t_c and this constitutes one gear mesh cycle.

In this article, the gear mesh is modelled as both a linear (LTV) and a non-linear time-varying (NLTV) system. First, friction is included as an LTV parameter and the harmonic balance method (HBM) is applied to analyze the dynamic response. Then, an analytical model is presented which incorporates the non-linearities due to the friction phenomenon. Subsequently, numerical techniques are applied to estimate the response of the system under miscellaneous conditions. Parametric studies are carried out to demonstrate the significance of friction in the overall dynamic response and stability of the system. The specific objectives of this paper are to: (1) develop a non-linear gear dynamic model incorporating sliding friction, (2) study effects of non-linearities on dynamic behavior of a spur gear pair, (3) compare LTV and NLTV models, (4) construct semi-analytical solutions for friction mechanism using HBM, (5) examine system stability issues, and (6) compare non-linear friction and equivalent viscous damping models.

In order to accentuate the non-linear and parametric effects of sliding at the teeth, a simplified model is developed with several underlying assumptions. Only the torsional motion of the gears is considered, which assumes that all mountings are rigid and auxiliary components such as the driving inertias and shafts are ignored. Mesh stiffness is assumed to follow a simplified periodic variation in the form of rectangular pulses. The coefficient of friction, while considered to be an idealized function of the surface sliding speed, is modelled to be independent of other operating conditions. Furthermore, the normal contact load is assumed to be equally distributed amongst all the teeth in contact, under both static and dynamic conditions. For this gear pair, other non-linearities such as the ones arising due to tooth backlash and spatial domain dependency of mesh stiffness are neglected.

3. TRIBOLOGICAL CONSIDERATIONS

Sliding on the gear tooth surface causes a frictional force F_f along the off-line of action direction, which is designated as the η-axis. As the gears roll, the tooth interface point moves along the contact line or the line of action (ξ direction). These linearly varying values of $\xi_p(t)$ and $\xi_g(t)$ result in a time-varying torque T_f about the two gear axes, which will also depend upon the coefficient of friction and the normal load. Till this instant t_a, the sliding velocity V_s on the two pairs of teeth is opposite in direction, and consequently, so is the friction force F_f. During the period, the net force in the η direction is zero; however, $T_f \neq 0$ due to the spacing between the gear teeth and hence the different points of application of these two friction forces. Subsequently, the directions of friction force as well as the torque reverse at the pitch point for each tooth.

Under typical running conditions, the gears operate in a regime of mixed lubrication [18, 19], characterized by partial asperity contact and a fluid film formation. The coefficient of friction μ is a complex function of many tribological parameters, as given by $\mu = f(V_S, N, V_R, T, R_q \ldots)$, where V_S and V_R are the sliding and rolling velocities respectively, N is the normal load at the tooth contact zone, T is the temperature and R_q is the compound surface roughness of the contact surfaces. For instance, one of the commonly used equations for estimating μ in a gear mesh was proposed by Kelley and Lemanski [18] as

$$\mu = C_1 \frac{1}{1 - C_3 R_q} \log_{10} \left[\frac{C_2 w}{\eta_0 V_S V_t^2 (\rho_p + \rho_g)^2} \right]. \tag{1}$$

Here, C_1, C_2 and C_3 are empirical coefficients that depend upon the applied units, ρ_p and ρ_g are the local radii of curvature of pinion and gear respectively, w is the load distribution per unit length and η_0 is the dynamic viscosity of the lubricant. Equation (1) predicts a considerable variation in the value of μ during a complete mesh cycle. Nevertheless, recent studies [2, 19] have established that during one meshing cycle, changes in the magnitude of the coefficient of friction are less significant when compared with the effect of the reversal of sign at the pitch point. Hence, the exact variation of μ may be ignored for simplicity and it can be represented by the Coulomb model. For each tooth pair i in contact

$$\mu_i = \mu_0 \operatorname{sgn}(V_{S,i}) \tag{2}$$

where

$$\operatorname{sgn}(V) = \begin{cases} +1, & V > 0, \\ 0, & V = 0, \\ -1, & V < 0. \end{cases}$$

Here V_s is the relative sliding velocity between the two mating surfaces for any given pair of teeth and μ_0 is the coefficient of friction for the interface, which is a material property of contacting surfaces. An alternative, yet analytical, representation using a trigonometric function is proposed below, so that the discontinuity at the pitch point is avoided.

$$\mu_i = \frac{2}{\pi} \mu_0 \tan^{-1}(V_{S,i}/V_0). \tag{3}$$

In equation (3), V_0 is introduced as a reference velocity used for non-dimensionalization of sliding speed. Additionally, it controls the degree of non-linearity near the pitch point, when the sign of V_S reverses. The lower the value of V_0, the higher is the slope of the

trigonometric function and hence the function tends towards a closer approximation to the Signum function given by equation (2). For gear applications, which have combined rolling–sliding conditions, the rolling velocity V_R can be a logical choice for the value of V_0 in equation (3).

4. LINEAR TIME-VARYING SYSTEM MODEL

Previous analytical studies [2–7] have considered the friction between gear teeth as a time-varying function, such that the sliding velocity is determined solely from the kinematic considerations. This assumption has been found to be valid under non-resonant conditions, when the vibratory component of angular velocity of the gears is much smaller as compared to the mean angular rotational speed. Furthermore, all meshing parameters such as stiffness, damping and moment arm ξ are also assumed to be explicit functions of time. Table 1 shows the representative design for a gear pair example studied in this paper. The assumed idealized variations in these parameters within a mesh cycle are shown in Figure 2.

A problem thus defined assumes the form of a linear time-varying system and the equations of torsional motion can be written as follows (subscripts p and g stand for the pinion and gear respectively):

$$J_p\ddot{\theta}_p + c(t)\,(\dot{\theta}_p R_p - \dot{\theta}_g R_g - \dot{\varepsilon})\,R_p + k(t)(\theta_p(t)R_p - \theta_g(t)R_g - \varepsilon(t))R_p = T_p + \sum_i \mu_i(t)N_i(t)\xi_i(t), \tag{4}$$

$$J_g\ddot{\theta}_g + c(t)(\dot{\theta}_g R_g - \dot{\theta}_p R_p + \dot{\varepsilon})\,R_g + k(t)(\theta_g(t)R_g - \theta_p(t)R_p + \varepsilon(t))R_g = -T_g - \sum_j \mu_j(t)N_j(t)\xi_j(t). \tag{5}$$

Here J is the moment of inertia, R is the base radius of the corresponding gear, ε is the unloaded static transmission error and i and j are the indices of the particular teeth in contact. In this form, equations (4) and (5) constitute a semi-definite system, and these can be reduced to a single equation by defining the dynamic transmission error (DTE) as $\delta(t) = R_p\theta_p(t) - R_g\theta_g(t)$:

$$J_p J_g\ddot{\delta} + c(t)(\dot{\delta} - \dot{\varepsilon})(R_p^2 J_g + R_g^2 J_p) + k(t)(\delta(t) - \varepsilon(t))(R_p^2 J_g + R_g^2 J_p) = (T_p R_p J_g + T_g R_g J_p) + J_g R_p \sum_i \mu_i(t)N_i(t)\xi_i(t) + J_p R_g \sum_j \mu_j(t)N_j(t)\xi_j(t). \tag{6}$$

TABLE 1

Gear design parameters and critical time instant values for one mesh cycle

Number of teeth Π_p, Π_g	25, 31	Input torque T_p	226 Nm
Center distance	88·9 mm	k_{mean} (N/m)	5·68e8
Profile contact ratio Γ	1·433	k_{max} (N/m)	7·20e8
Input speed Ω_p	1500 rpm	k_{max}/k_{min}	1·667
Lowest point of single tooth contact (t_a)		0·693 ms	
Pitch point (t_b)		1·148 ms	
Highest point of single tooth contact (t_c)		1·600 ms	

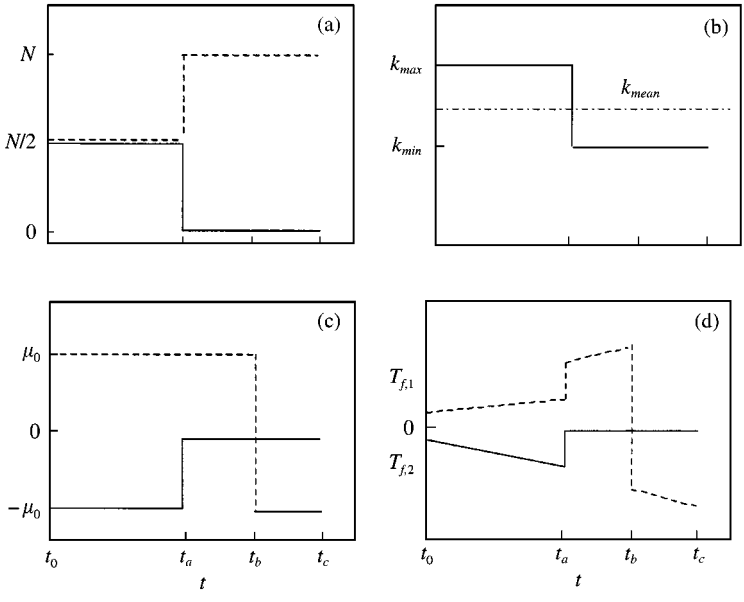

Figure 2. Assumed periodic meshing parameters during one meshing cycle: ——, 1st tooth; - - -, 2nd tooth. (a) Load distribution function $N(t)$; (b) total mesh stiffness $k(t)$; (c) coefficient of the friction μ, and (d) friction torque $T_F(t)$.

Furthermore, the normal force at the gear teeth can be defined either on the basis of a load distribution under quasi-static conditions, or that due to the actual tooth load under dynamic conditions. These two cases have been analyzed by the authors in an earlier paper [7] using Floquet theory. It was shown that the application of dynamic tooth load has only a marginal effect on the dynamic response.

5. SEMI-ANALYTICAL MODEL FOR THE LTV SYSTEM

5.1. PROBLEM FORMULATION

The multi-term harmonic balance method (HBM) is first applied to this problem for the case with quasi-static load distribution, since this method could be extended to non-linear systems. Equation (6) can be written as

$$\frac{J_e}{J_b}\ddot{\delta} + c(t)(\dot{\delta} - \dot{\varepsilon}) + k(t)(\delta(t) - \varepsilon(t))$$

$$= \frac{T_{eq}}{J_b} + \frac{J_g R_p}{J_b}\sum_i \mu_i(t) N_i(t)\xi_i(t) + \frac{J_p R_g}{J_b}\sum_j \mu_j(t) N_j(t)\xi_j(t). \tag{7}$$

Here, the following equivalent factors have been used:

$$T_{eq} = J_g R_p T_p + J_p R_g T_g, \qquad J_b = J_g R_p^2 + J_p R_g^2, \qquad J_e = J_p J_g. \tag{8a–c}$$

Using equations (7) and (8), the viscous damping ratio ζ can be defined as

$$\zeta = \frac{c}{2}\sqrt{\frac{J_b}{kJ_e}}. \tag{9}$$

The solution is assumed to contain the first three harmonics (ω_0, $2\omega_0$ and $3\omega_0$) of the tooth meshing frequency ω_0:

$$\delta_h(t) = a_{\delta 0} + \sum_{i=1}^{n_h} a_{\delta i}\cos(\mathrm{i}\omega_0 t) + \sum_{i=1}^{n_h} b_{\delta i}\sin(\mathrm{i}\omega_0 t). \tag{10}$$

Additionally, the first and third super-harmonics of the first sub-harmonic term (i.e., $0{\cdot}5\omega_0$ and $1{\cdot}5\omega_0$) are also included. Thus, the sub-harmonic component of the dynamic transmission error $\delta_u(t)$ and the total transmission error $\delta(t)$ can be expressed as

$$\delta_u(t) = \sum_{i=1}^{n_u} c_{\delta i}\cos((\mathrm{i} - 0{\cdot}5)\omega_0 t) + \sum_{i=1}^{n_u} d_{\delta i}\sin((\mathrm{i} - 0{\cdot}5)\omega_0 t), \tag{11}$$

$$\delta(t) = \delta_h(t) + \delta_u(t). \tag{12}$$

Each of the time-varying parameters, namely stiffness, damping, coefficient of friction and static unloaded transmission error is also expanded by Fourier series up to three harmonic terms. For example, the Fourier coefficients of stiffness are shown in equation (13). The Fourier expansion for viscous damping terms will be similar to these since damping is assumed to follow the same form of variation:

$$a_{k0} = \frac{1}{t_c}[k_{max}(t_a) + k_{min}(t_c - t_a)], \qquad a_{ki} = \frac{1}{\pi i}(k_{max} - k_{min})\sin\frac{2\pi i t_a}{t_c},$$

$$b_{ki} = \frac{k_{max} - k_{min}}{\pi i}\left(1 - \cos\frac{2\pi i t_a}{t_c}\right). \tag{13a–c}$$

For the friction expression, all terms with the combined product $\mu(t)N(t)\xi(t)$ are collected and their Fourier coefficients are given by equation (14). The transmission error $\varepsilon(t)$ is assumed to be already in the form of a summation of sine series. Note that all of these terms have the same periodicity of one tooth meshing cycle

$$a_{f0} = \frac{1}{t_c}\left[D_1 t_a + \frac{(D_2 + D_3)(t_b - t_a)}{2} + \frac{(D_4 + D_5)(t_c - t_b)}{2}\right]. \tag{14a}$$

$$\begin{aligned} a_{fi} = {} & \frac{1}{\pi i}\left[D_1 \sin\frac{2\pi i t_a}{t_c}\right] + \left(\frac{D_2 t_b - D_3 t_a}{t_b - t_a}\right)\frac{1}{\pi i}\left[\sin\frac{2\pi i t_b}{t_c} - \sin\frac{2\pi i t_a}{t_c}\right] \\ & + \left(\frac{D_4 t_c - D_5 t_b}{t_c - t_b}\right)\frac{1}{\pi \mathrm{i}}\left[-\sin\frac{2\pi i t_b}{t_c}\right] + \left(\frac{D_3 - D_2}{t_b - t_a}\right)\frac{1}{\pi i}\left[t_b \sin\frac{2\pi i t_b}{t_c} - t_a \sin\frac{2\pi i t_a}{t_c}\right] \\ & + \left(\frac{D_5 - D_4}{t_c - t_b}\right)\frac{1}{\pi \mathrm{i}}\left[-t_b \sin\frac{2\pi i t_b}{t_c}\right] + \left(\frac{D_3 - D_2}{t_b - t_a}\right)\frac{t_c}{2\pi^2 i^2}\left[\cos\frac{2\pi i t_b}{t_c} - \cos\frac{2\pi i t_a}{t_c}\right] \\ & + \left(\frac{D_5 - D_4}{t_c - t_b}\right)\frac{t_c}{2\pi^2 i^2}\left[1 - \cos\frac{2\pi i t_b}{t_m}\right], \end{aligned} \tag{14b}$$

$$b_{fi} = \frac{1}{\pi i}\left[D_1\left(1 - \cos\frac{2\pi i t_a}{t_c}\right)\right] + \left(\frac{D_2 t_b - D_3 t_a}{t_b - t_a}\right)\frac{1}{\pi i}\left[\cos\frac{2\pi i t_a}{t_c} - \cos\frac{2\pi i t_b}{t_c}\right]$$

$$+ \left(\frac{D_4 t_c - D_5 t_b}{t_c - t_b}\right)\frac{1}{\pi i}\left[\cos\frac{2\pi i t_b}{t_c} - 1\right] + \left(\frac{D_3 - D_2}{t_b - t_a}\right)\frac{1}{\pi i}\left[t_a \cos\frac{2\pi i t_a}{t_c} - t_b \cos\frac{2\pi i t_b}{t_c}\right]$$

$$+ \left(\frac{D_5 - D_4}{t_c - t_b}\right)\frac{1}{\pi i}\left[t_b \cos\frac{2\pi i t_b}{t_c} - 1\right] + \left(\frac{D_3 - D_2}{t_b - t_a}\right)\frac{t_c}{2\pi^2 i^2}\left[\sin\frac{2\pi i t_b}{t_c} - \sin\frac{2\pi i t_a}{t_c}\right]$$

$$+ \left(\frac{D_5 - D_4}{t_c - t_b}\right)\frac{t_c}{2\pi^2 i^2}\left[-\sin\frac{2\pi i t_b}{t_m}\right], \tag{14c}$$

where D_1–D_5 are given as follows; L_c represents the length of the line of action of the gear pair, α is the roll angle of the pinion and α_m is the angular pitch of the pinion.

$$D_1 = \frac{1}{2J_b}\left[(J_p R_g - J_g R_p)\,\mu_0 N \alpha_m R_p\right], \tag{15a}$$

$$D_2 = \frac{\mu_0 N}{J_b}\left[J_g R_p^2 \alpha_a + J_p R_g (L_c - R_p \alpha_a)\right], \tag{15b}$$

$$D_3 = \frac{\mu_0 N}{J_b}\left[J_g R_p^2 \alpha_b + J_p R_g (L_c - R_p \alpha_b)\right], \tag{15c}$$

$$D_4 = -D_3, \qquad D_5 = -\frac{\mu_0 N}{J_b}\left[J_g R_p^2 \alpha_c + J_p R_g (L_c - R_p \alpha_c)\right]. \tag{15d, e}$$

5.2. SOLUTIONS FROM THE HARMONIC BALANCE METHOD

To find the solution, expressions in equations (13)–(15) are substituted into equations (10)–(12). Then after balancing the terms corresponding to the first three harmonics in the governing equation (7), the following matrix relationship is obtained.

$$\left[K_h(\omega)\right]\begin{Bmatrix} a_{\delta 0} \\ a_{\delta 1} \\ a_{\delta 2} \\ a_{\delta 3} \\ b_{\delta 1} \\ b_{\delta 2} \\ b_{\delta 3} \end{Bmatrix} = \{F(\omega)\}. \tag{16}$$

Here, $K_h(\omega)$ is a 7×7 matrix consisting of stiffness and damping terms. Similarly, $F(\omega)$ is the equivalent force vector comprising profile errors, external load and friction terms.

TABLE 2

Fourier coefficients of parameters in the gear mesh system for baseline values

	Stiffness k (MN/m)		Viscous damping c (Ns/m)		Profile error ε (μm)		Friction term (N)	
Mesh harmonic	a_k	b_k	a_c	b_c	a_e	b_e	a_f	b_f
0th (mean)	556·7		518·2		0		−12·9	
1st	37·4	175	17·4	81·5	0·356	1·75	−223	34·3
2nd	−34·1	15·2	−15·9	7·08	0·063	−0·048	70·7	164
3rd	29·1	39·9	13·5	18·6	0·077	0·123	20·5	−15·2

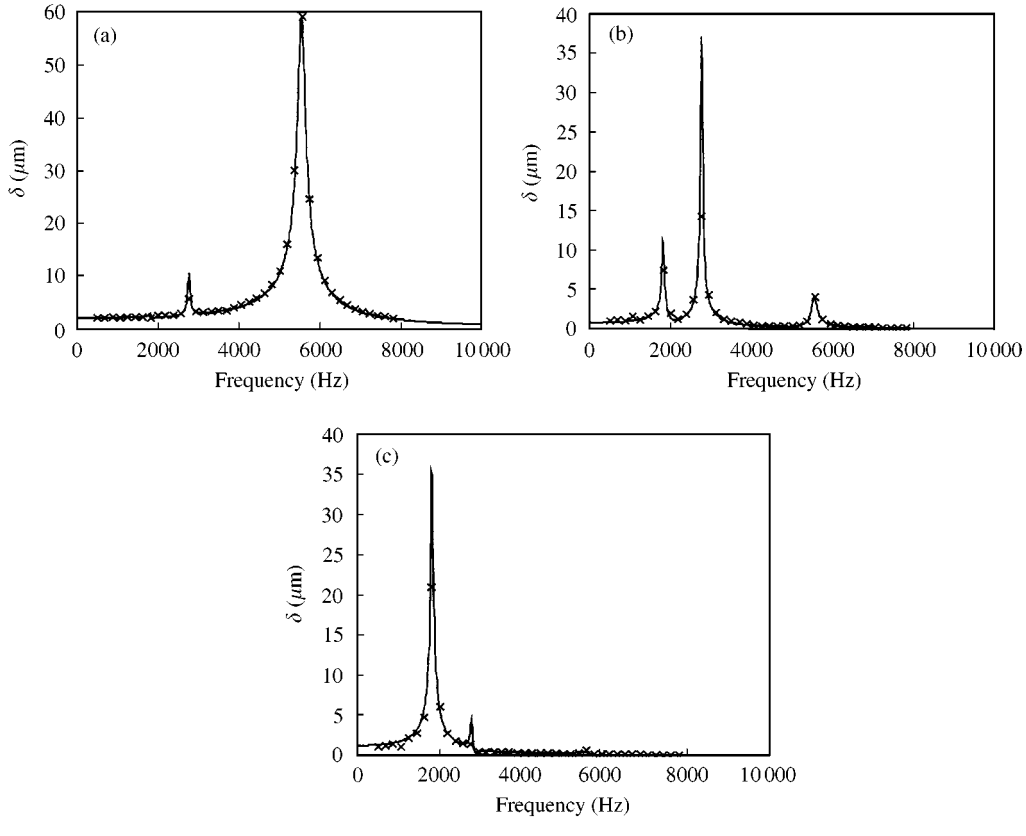

Figure 3. Comparison of semi-analytical and numerical solutions for LTV gear system: ×, simulation; ——, HBM. (a) First harmonic of gear mesh frequency; (b) second harmonic; (c) third harmonic.

Equation (16) can now be applied in order to solve for the coefficients of the dynamic transmission error terms by computing the inverse of the $K_h(\omega)$ matrix at any frequency ω. The term $a_{\delta 0}$ appears as the mean deflection due to the external time-variant torque. Equations (17) and (18) show the first row of the equation in its expanded form. Here, a and b represent the cosine and sine coefficients of Fourier series expansion. Subscripts k, c, e and

f stand for stiffness, viscous damping, profile error and friction, respectively, and the numerical subscripts 0–3 indicate the order of the fundamental mesh harmonic. Typical values of these coefficients are listed in Table 2.

$$F_1 = (b_{k1}\,b_{e1} + b_{k3}\,b_{e3} + a_{k1}\,a_{e1} - 3\omega b_{c3}a_{e3} + a_{k2}a_{e2} + 3\omega a_{c3}b_{e3} + 3\omega a_{c1}b_{e1})/2 + T_{eq}/J_b + b_{k2}b_{e2} + f_0/J_b + \omega a_{c2}b_{e2} + k_0e_0 + a_{k3}a_{e3} - \omega b_{c2}a_{e2} - \omega b_{c1}a_{e1}, \quad (17)$$

$$A_{1,1:7} = \left[k_0 \frac{-\omega b_{c1} + a_{k1}}{2} - \omega b_{c2} + \frac{a_{k2}}{2} \frac{-3\omega b_{c3} + a_{k3}}{2} \frac{b_{k1} + \omega a_{c1}}{2} \omega a_{c2} + \frac{b_{k2}}{2} \frac{b_{k3} + 3\omega a_{c3}}{2} \right]. \quad (18)$$

Figure 3 presents the magnitude $|\delta| = \sqrt{a_{\delta i}^2 + b_{\delta i}^2}$ at the first three harmonics as a function of the excitation frequency ($f_0 = \omega_0/2\pi$) for the gear design and operating conditions described in Table 1. The natural frequency of the system is 5·6 kHz corresponding to the largest peak in the response function in Figure 3(a). The peaks at 2·8 and 1·9 kHz represent the first and the second super-harmonic response. These results are compared with the values obtained from numerical integration. There is a good match for the first harmonic, but the errors grow for higher harmonics. Hence the harmonic balance method can be applied to predict the dynamic response of LTV gear systems under the influence of friction, but the accuracy of predictions would depend upon the number of frequency terms considered in the solution.

5.3. ANALYSIS OF SUB-HARMONIC RESPONSE

Next, the sub-harmonic response is considered by gathering the terms corresponding to $0{\cdot}5\omega_0$ (subscript 1) and $1{\cdot}5\omega_0$ (subscript 2). In equation (19), c and d represent the cosine and sine terms respectively. There is no external excitation at these frequencies, hence the right-hand side of equations is simply a null vector.

$$[K_u(\omega)] \begin{Bmatrix} c_{\delta 1} \\ c_{\delta 2} \\ d_{\delta 1} \\ d_{\delta 2} \end{Bmatrix} = \begin{Bmatrix} 0 \\ 0 \\ 0 \\ 0 \end{Bmatrix}. \quad (19)$$

The various terms in the matrix K_u are as follows:

$$[K_u(\omega)] = [K_1(\omega)\,;K_2(\omega)] \quad (20a)$$

$$[K_1(\omega)] = \left[\begin{array}{cc} -\frac{\omega^2 J_e}{4J_b} - \frac{\omega b_{c1}}{4} + k_0 + \frac{a_{k1}}{2} & -\frac{3\omega b_{c1}}{4} - \frac{3\omega b_{c2}}{4} + \frac{a_{k1}}{2} + \frac{a_{k2}}{2} \\ -\frac{\omega b_{c1}}{4} - \frac{\omega b_{c2}}{4} + \frac{a_{k1}}{2} + \frac{a_{k2}}{2} & -\frac{9\omega^2 J_e}{4J_b} - \frac{3\omega b_{c3}}{4} + k_0 + \frac{a_{k3}}{2} \\ -\frac{\omega c_0}{2} + \frac{\omega a_{c1}}{4} + \frac{b_{k1}}{2} & -\frac{3\omega a_{c1}}{4} + \frac{3\omega a_{c2}}{4} - \frac{b_{k1}}{2} + \frac{b_{k2}}{2} \\ \frac{\omega a_{c2}}{4} - \frac{\omega a_{c1}}{4} + \frac{b_{k1}}{2} + \frac{b_{k2}}{2} & -\frac{3\omega c_0}{2} + \frac{3\omega a_{c3}}{4} + \frac{b_{k3}}{2} \end{array}\right], \quad (20b)$$

$$[K_2(\omega)] = \left[\begin{array}{cc:c} -\frac{\omega c_0}{2} + \frac{\omega a_{c1}}{4} + \frac{b_{k1}}{2} & & \frac{\omega a_{c2}}{4} - \frac{\omega a_{c1}}{4} + \frac{b_{k1}}{2} + \frac{b_{k2}}{2} \\ -\frac{3\omega a_{c1}}{4} + \frac{3\omega a_{c2}}{4} - \frac{b_{k1}}{2} + \frac{b_{k2}}{2} & & -\frac{3\omega c_0}{2} + \frac{3\omega a_{c3}}{4} + \frac{b_{k3}}{2} \\ -\frac{\omega^2 J_e}{4J_b} + \frac{\omega b_{c1}}{4} + k_0 - \frac{a_{k1}}{2} & & -\frac{3\omega b_{c1}}{4} + \frac{3\omega b_{c2}}{4} + \frac{a_{k1}}{2} - \frac{a_{k2}}{2} \\ \frac{\omega b_{c1}}{4} + \frac{\omega b_{c2}}{4} + \frac{a_{k1}}{2} - \frac{a_{k2}}{2} & & -\frac{9\omega^2 J_e}{4J_b} + \frac{3\omega b_{c3}}{4} + k_0 - \frac{a_{k3}}{2} \end{array}\right]. \quad (20c)$$

For this homogenous set of equations to have a non-trivial solution, the matrix K_u must be singular. Such points correspond to period-doubling instability [11, 20–22] and will be found by computing the determinant of K_u as a function of excitation frequency. Figure 4 shows the plot of $\det(K_u)$ for four different values of the damping ratio ζ. The points of intersection with the abscissa indicate the onset of instability. Thus, the first period doubling will occur when ζ is less than 0·05, whereas the period doubling of the third harmonic occurs for damping values less than 0·01. Figure 5 shows the actual system response for values chosen from these graphs, as well as different damping values.

Figure 5(a) shows the frequency spectrum of the dynamic transmission error δ when the excitation frequency lies near the second sub-harmonic of the gear system, i.e., $\omega_0 \approx 2\omega_n/3$, resulting in an unstable response with strong sub-harmonics. A minor shift in excitation frequency results in a stable response with no sub-harmonics, as shown in Figure 5(b). Similarly, Figure 5(c) and 5(d) shows the influence of damping on the system at the first sub-harmonic, where $\omega_0 \approx 2\omega_n$. These graphs show that a change in damping ratio from 0·01 to 0·05 can affect the stability of the system significantly.

5.4. EFFECTS OF KEY PARAMETERS

The method of harmonic balance can be applied to conduct a parametric study of the gear system. Figure 6(a) shows the system response for the baseline conditions, as given in

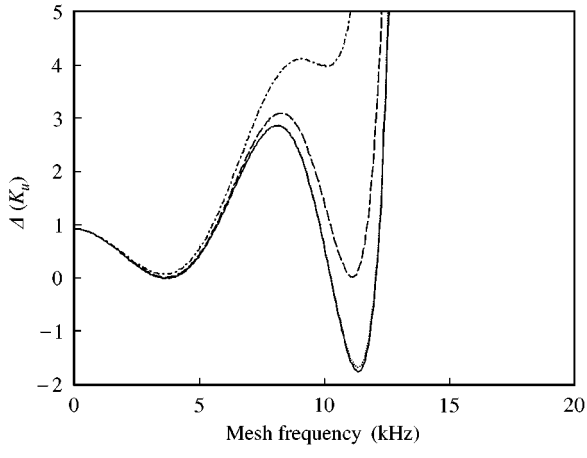

Figure 4. Determinant of matrix K_u as a function of gear mesh excitation frequency f_0: ——, $\zeta = 0$; · · · ·, $\zeta = 0{\cdot}01$; - - -, $\zeta = 0{\cdot}05$; · – · – ·, $\zeta = 0{\cdot}1$.

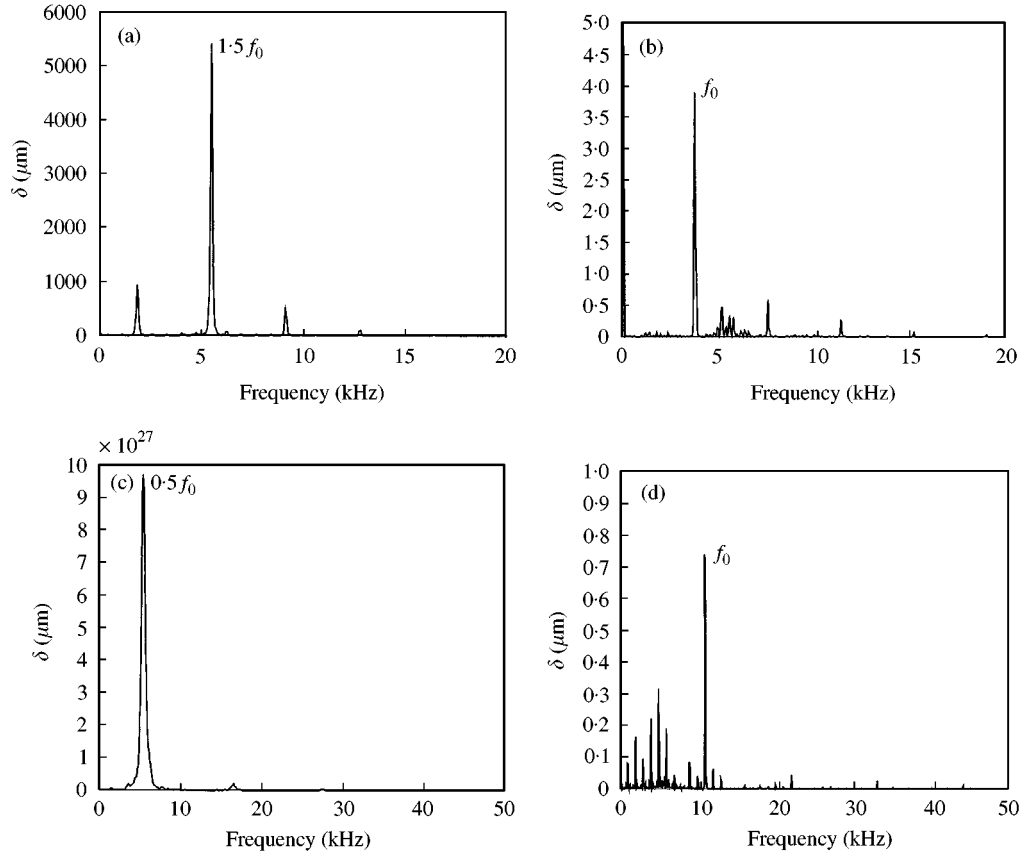

Figure 5. System response in terms of DTE for different values of damping and excitation frequencies: (a) $f_0 = 3{\cdot}65$ kHz, strong sub-harmonic zone; (b) $f_0 = 3{\cdot}8$ kHz, no sub-harmonic response; (c) $f_0 = 11{\cdot}0$ kHz, $\zeta = 0{\cdot}01$, unstable sub-harmonic response; (d) $f_0 = 11{\cdot}0$ kHz, $\zeta = 0{\cdot}05$, weak sub-harmonic response.

Table 1 with $\mu = 0{\cdot}1$ and $\zeta = 0{\cdot}01$. Figure 6(b) shows the response for the frictionless case, i.e., when $\mu = 0$. The difference between Figure 6(a) and 6(b) represents the contribution of friction to the total dynamic response. Note that the peaks corresponding to 2·8 kHz (second harmonic) have been affected the most. In Figure 6(c), the unloaded static transmission error ε is neglected and the dynamic response now jumps up since the profile modifications are designed to partly nullify the parametric variations in stiffness.

Finally, the contact ratio Γ is modified (Figure 6(d)) which leads to a change in mean stiffness according to the relationship

$$k_{mean} = \langle k(t) \rangle_t = \frac{1}{t_c} \int_0^{t_c} k(t)\,\mathrm{d}t = k_{max}(\Gamma - 1) + k_{min}(-\Gamma + 2). \tag{21}$$

Accordingly, the resonance peaks shift towards the right-hand side of the graph with increasing values of Γ. With this analysis, the effect of various individual excitations and parameters can be isolated, and their dynamic interactions can be studied. Furthermore, the harmonic balance method can be used to predict the sub-harmonic instabilities in the gear system.

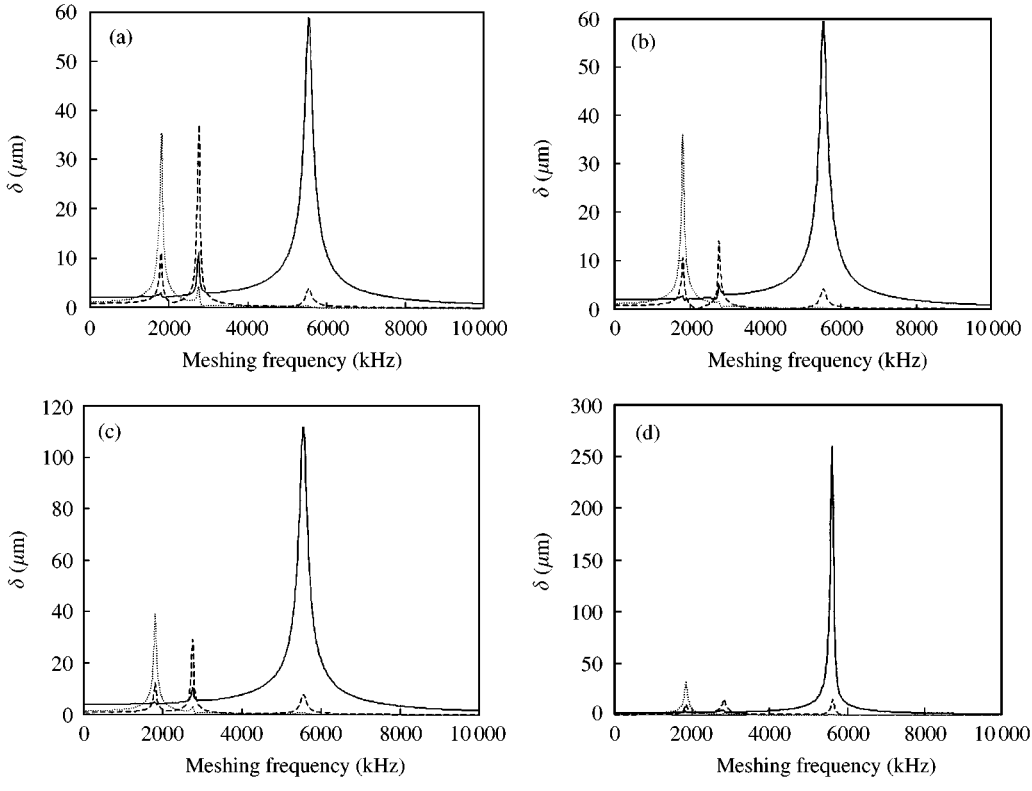

Figure 6. Effects of critical parameters on dynamic transmission error using HBM analysis: ——, 1st harmonic of gear mesh frequency f_0; - - -, 2nd harmonic; ····, 3rd harmonic. (a) Baseline values from Table 1; (b) $\mu = 0$; (c) $\varepsilon = 0$; (d) $\Gamma = 1{\cdot}4924$.

6. THE NON-LINEAR TIME-VARYING FORMULATION

6.1. INCIDENCE OF FRICTION NON-LINEARITY

In the preceding sections, the gear pair was analyzed with an LTV model of sliding friction, such that μ is an explicit function of time. Clearly, friction modelled in this manner has the primary effect of an external excitation, and would not accommodate the dissipative property of sliding resistance. In order to incorporate this aspect, the total instantaneous sliding velocity must be considered. This velocity would include the quasi-static value of angular speed as well as the vibratory component. When modelled in this manner, the friction mechanism exhibits an implicit non-linearity, where the resistive force is a function of the instantaneous surface velocity, which in turn is a system response variable. The coefficient of friction μ will now be determined by

$$\mu(t, \dot{\theta}_p, \dot{\theta}_g) = \operatorname{sgn}(V_S) = \operatorname{sgn}[\xi_g(t)(\Omega_g + \dot{\theta}_g(t)) - \xi_p(t)(\Omega_p + \dot{\theta}_p(t))]. \tag{22}$$

Equation (22) cannot be written explicitly in terms of a single variable δ. In order to completely define this system, at least two independent variables must be chosen from θ_p, θ_g and δ. This is contrary to LTV systems where the two equations reduce to a single equation with only one unknown parameter, as shown in equation (6). However, the system is still semi-definite and a stable solution for θ_p or θ_g may not be obtained. To resolve this

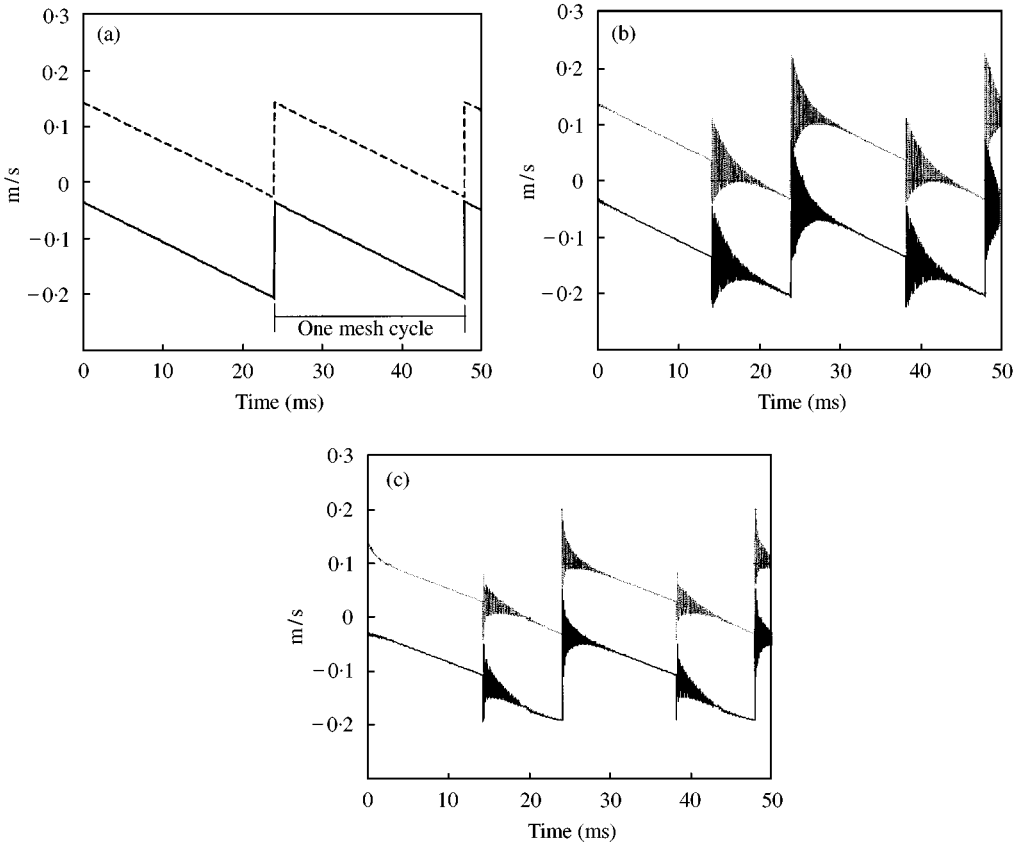

Figure 7. Sliding velocity variation for different modelling considerations: (a) under quasi-static conditions; (b) dynamic LTV model; (c) dynamic NLTV model with $\mu_0 = 0{\cdot}1$ ——, 1st tooth; - - -, 2nd tooth.

conflict, two alternative methods are suggested. In the first approach, one of the gears is fixed to the base via a torsional spring, thus making the system positive definite. This also leads to a system consistent with the energy conservation principle [15, 19]. In the second method, which may only be applied in numerical simulation, the equations are solved for the two angular displacement parameters θ_p and θ_g. Then a high-pass high-order digital filter may be applied to both the parameters, so that the displacement and velocity corresponding to the rigid body motion are disregarded. This dynamic component of the velocity is then used in equation (22) for calculating the coefficient of friction.

The difference between LTV and NLTV considerations can be seen from the corresponding plots of sliding velocity V_s within a mesh cycle. The relevant equations of motion are similar to equations (4) and (5), except that μ is now also a function of the instantaneous angular velocities, in addition to being a time-varying parameter. Figure 7 shows the result for V_s for the two teeth in contact under three different circumstances. In Figure 7(a), V_s is calculated using only the mean angular velocities Ω_p and Ω_g and the linearly varying distance ξ_p and ξ_g. Consequently, the variation in V_s shows straight lines with constant slope. The zero crossing point indicates the contact zone passing through the pitch point, where pure rolling occurs. Also note that although two teeth are in contact for a certain period, only one tooth passes through the $V_s = 0$ point. Figure 7(b) shows the dynamic variation in V_s, when the LTV model is used. Due to vibratory oscillations, there are multiple occurrences of pitch point crossing within a mesh cycle.

Furthermore, even tooth 2 goes through the point of $V_s = 0$. In the non-linear model, each zero crossing on the V_s plot is associated with the reversal in the sign of friction force, and hence it will impart significant energy dissipation to the system. Consequently, the magnitude of vibrations is considerably reduced for this regime, as seen in Figure 7(c).

6.2. SOLUTION METHODOLOGY

For the problem thus formulated in a non-linear time-varying form, analytical solutions are mostly precluded by the complexity of the equations, in particular due to the terms comprising friction elements. Blankenship and Singh [8] assumed that for a non-linear gear pair, the stability can largely be determined by the response at the first harmonic of the excitation frequency. Such a hypothesis clearly does not hold when a significant periodic variation is also present. Consequently, a higher order multi-term harmonic balance must be employed. For this, one may proceed in the following manner. Define the friction torque T_f and μ as

$$T_{f,i}(t, \dot{\theta}_p, \dot{\theta}_g) = \mu_i(t, \dot{\theta}_p, \dot{\theta}_g)\xi_{p,i}(t)N_i(t), \tag{23}$$

$$\mu_i(t, \dot{\theta}_p, \dot{\theta}_g) = \operatorname{sgn}\left(\frac{V_{s,i}}{V_R}\right) = \operatorname{sgn}\left[\frac{\xi_{g,i}(t)(\Omega_g + \dot{\theta}_g) - \xi_{p,i}(t)(\Omega_p + \dot{\theta}_p)}{V_R}\right]. \tag{24}$$

Furthermore, parameters ξ and θ are periodic within a meshing cycle and hence can be represented by their Fourier components. Thus, the expression for the friction torque becomes

$$T_f(t) = \operatorname{sgn}\left[\begin{array}{l}\left(\sum_{m=0}^{n_{\xi g}} \tilde{a}_{\xi g,m} e^{j\omega mt}\right)\left(\Omega_g + \sum_{m=0}^{n_{\theta g}} \tilde{a}_{\theta g,m} jm\omega e^{j\omega mt}\right) \\ \quad - \left(\sum_{m=0}^{n_{\xi p}} \tilde{a}_{\xi p,m} e^{j\omega mt}\right)\left(\Omega_p + \sum_{m=0}^{n_{\theta p}} \tilde{a}_{\theta p,m} jm\omega e^{j\omega mt}\right)\end{array}\right]$$

$$\times\left[\sum_{m=0}^{n_{\xi p}} \tilde{a}_{\xi p,m} e^{j\omega mt}\right]\left[\sum_{m=0}^{n_N} \tilde{a}_{N,m} e^{j\omega mt}\right]. \tag{25}$$

Here, n is the number of terms considered in Fourier expansion and $\tilde{a}$ is the complex-valued Fourier amplitude for the corresponding parameter. Furthermore, the signum function can be expressed in its Fourier form as follows [23]:

$$\operatorname{sgn}(x) = \frac{4}{\pi}\left[\sum_{m=0}^{n_u} \frac{\sin(2m+1)x}{2m+1}\right]. \tag{26}$$

This will lead to fifth order products in the multiharmonic terms, whose numbers will further multiply when sub-harmonic response is also considered. Additionally, the non-linear system comprises two simultaneous equations and the number of terms will increase accordingly. For example, if n harmonic terms are considered in the solution, then the number of terms in the expanded equation is approximately $100(2n + 1)^7$. Thus, even if a single harmonic is considered, there will be $O(10^5)$ terms in the expression. Such a complex formulation is obviously intractable for the application of harmonic balance method.

6.3. DYNAMIC RESPONSE

Due to the complexities in analytical methods, the discussion of non-linear effects of friction is largely confined to solutions obtained using numerical integrations. In the current methodology, the two non-linear equations are solved simultaneously. For computing the instantaneous coefficient of friction, the angular velocities of pinion and gear are digitally filtered to obtain only the dynamic component. For the gear system described in Table 1, numerical simulation is carried out at very low rotational speed. Three different cases are analyzed and the results are shown in Figure 8 in terms of the dynamic transmission error δ.

First, the response is computed for the gear pair with no sliding friction at the teeth. Figure 8(a) distinctly shows the regions of mesh stiffness variations, but the pitch point on the gear tooth is indistinguishable due to the absence of friction. At each transition in the number of teeth in contact, there is an impulse-like excitation due to the sudden change in stiffness. Note that this is the result of the assumed $k(t)$ profile, as shown in Figure 2. Next, friction is included as an LTV parameter and now an additional excitation can be observed at the pitch point, as shown in Figure 8(b). Since a pseudo-Coulomb model of friction is used, the pitch point also undergoes an impulsive force, although with a somewhat smaller amplitude. When the same system is analyzed with non-linearities (Figure 8(c)), the oscillations at the pitch point result in multiple occurrences of reversal of sliding velocity direction at the pitch point, and the vibrations are dampened significantly. However, the rest of the graph largely remains unaffected. From these simulations, two important issues emerge; first, although non-linear effects in friction seem to have only a local influence in the

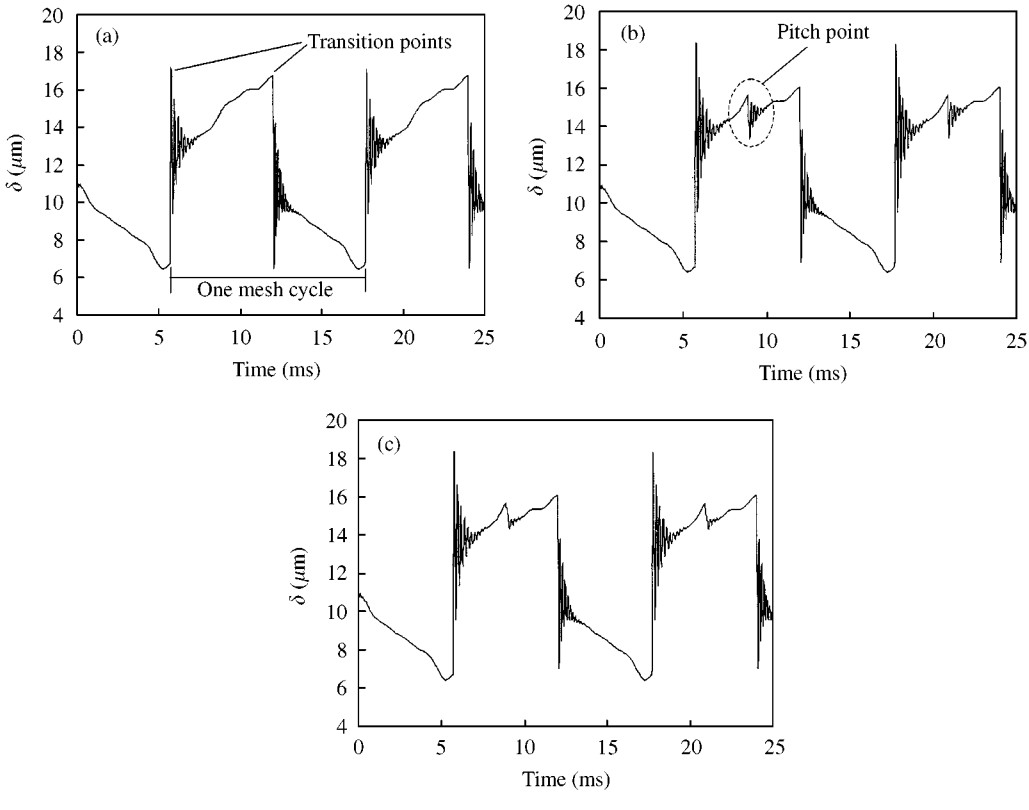

Figure 8. Dynamic response for the three friction models in terms of δ, $\Omega = 200$ rpm, $\zeta = 0{\cdot}05$: (a) LTV system with $\mu_0 = 0$; (b) LTV system with $\mu_0 = 0{\cdot}1$; (c) NLTV system with $\mu_0 = 0{\cdot}1$.

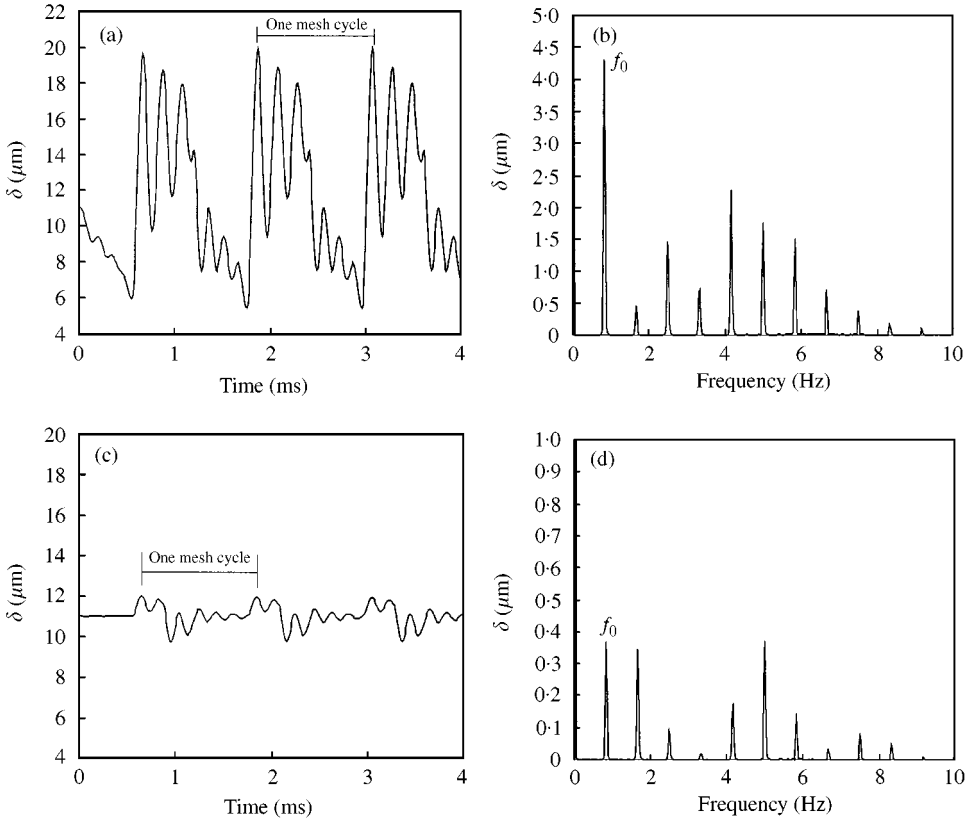

Figure 9. Contribution of friction to the overall dynamic response $\delta(t)$ for a non-linear system, at $\Omega = 2000$ rpm and $\zeta = 0{\cdot}05$: (a) time-domain response for combined excitation; (b) frequency spectrum for combined excitation; (c) time-domain response only due to friction excitation; (d) frequency spectrum only due to friction excitation.

time-domain, this situation may change near resonance conditions. Secondly, the positioning of the pitch point to the transition point is critical for determining the effects of friction on response. If the pitch point occurs immediately after the transition point, we can see that the damping effect in that case will be maximum.

Using the non-linear model developed, the influence of friction parameter is studied for a typical set of operating conditions. Figure 9(a) and 9(b) shows the time and frequency responses of the total system, and includes the parametric excitation, friction and input due to profile errors. In Figure 9(c) and 9(d), the profile errors are assumed to be zero and the time-varying mesh stiffness is replaced by its mean component. Thus, frictional torque is the only external excitation for this system. From this figure, it is apparent that as an excitation, friction is not a significant contributor to the whole system. However, the frequency spectrum shows that at some frequencies, especially for higher harmonics, its effect may be more apparent. This situation is highly dependent on the operating conditions though.

7. STABILITY ANALYSIS FOR THE NLTV SYSTEM

7.1. SLIDING FRICTION VERSUS VISCOUS DAMPING

Another characteristic of friction is the energy loss, which has led some researchers to treat the sliding resistance as an equivalent viscous damping element [4, 8]. To find such

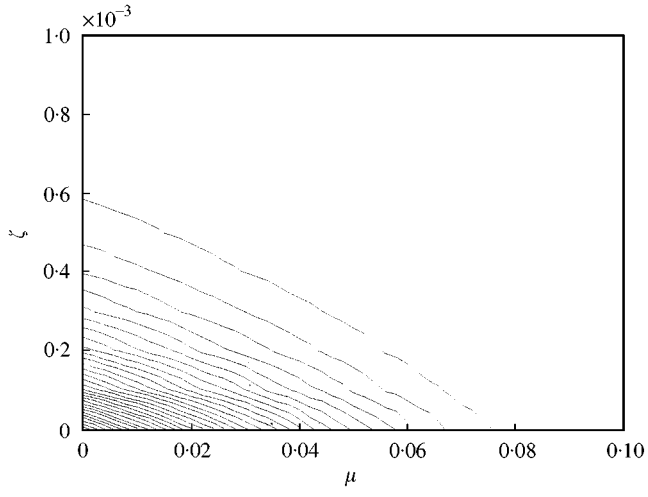

Figure 10. Contour plot of dynamic transmission error.

a relationship, the dynamic response is computed near resonance under three conditions: (1) with friction and no damping, (2) with damping and no friction, and (3) a combination of sliding friction and viscous damping. Figure 10 shows the contour plots for a given dynamic transmission error δ, where the damping ratio ζ is plotted along the abscissa and the ordinate represents the coefficient of friction. Each iso-amplitude curve represents the combination of μ and ζ that results in the same peak-to-peak dynamic transmission error. The negative sloping lines show an approximately linear relationship between the two parameters, i.e., $a_1\mu + a_2\zeta + a_3 = 0$. The equivalent value of ζ is somewhat small, which implies that the sliding friction has a rather weak influence as a viscous damping parameter. One possible explanation for this could be that the friction non-linearity is effective only for a small fraction of the total mesh cycle.

To further establish the damping characteristics of friction-induced non-linearities, the dynamic response is compared for LTV and NLTV systems. The profile error excitation ε is assumed to be zero in these plots. The initial state is defined by a stationary condition ($\dot{\delta} = 0$) and a static deflection based on the external mean load and time-averaged mesh stiffness. Figure 11 shows the dynamic response obtained by LTV analysis under non-resonant conditions, whereas Figure 12 shows the results from NLTV analysis under identical operating conditions. Clearly, the two responses are nearly the same, in both time and frequency domains. In this condition, the friction acts primarily as an excitation and hence does not demonstrate any difference between the two analyses.

Next, the contact ratio Γ is altered slightly and the damping ratio ζ is reduced to 0·001 in order to force the system into one of its unstable regimes. As a result, the LTV system in Figure 13 exhibits a divergent response for the dynamic transmission error, corresponding to saddle-node bifurcation instability. Subsequently, the gear pair is analyzed using the non-linear model of friction and the corresponding time-domain and frequency response is shown in Figure 14. Clearly, the system now exhibits long-term stability. It may be noted that the spectral ratios in Figures 13(b) and 14(b) are similar. On the contrary, a period-doubling instability would show entirely different spectra for the stable and unstable cases, as seen previously in the LTV analysis (see Figure 5). These results indicate that under certain circumstances, friction at the gear teeth may have a stabilizing effect on the gear system. Needless to say, this conclusion is only valid given the scope of our formulation where the clearance non-linearity has been ignored.

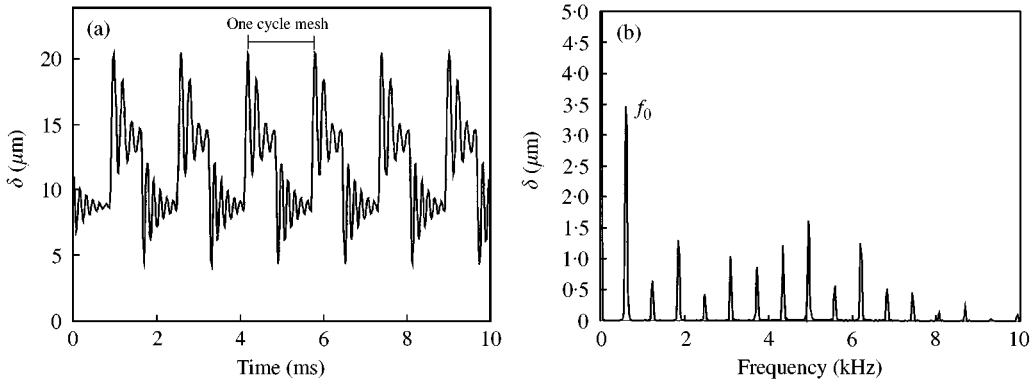

Figure 11. Dynamic response $\delta(t)$ with LTV analysis, away from resonance conditions for $\zeta = 0{\cdot}05$, $\mu = 0{\cdot}1$, $\Omega = 1490$ rpm, $\Gamma = 1{\cdot}532$: (a) time-domain response; (b) frequency spectrum.

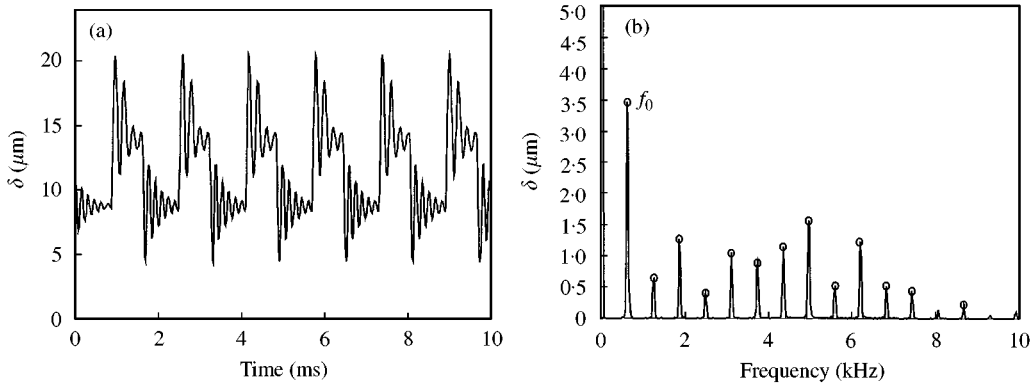

Figure 12. Dynamic response $\delta(t)$ with NLTV analysis, away from resonance conditions for $\zeta = 0{\cdot}05$, $\mu = 0{\cdot}1$, $\Omega = 1490$ rpm, $\Gamma = 1{\cdot}532$: (a) time-domain response; (b) frequency spectrum; ○, values from LTV analysis.

7.2. LTV VERSUS NLTV SYSTEMS

This analysis is extended over a wider range of running conditions. The dynamic response of the system is computed for several values of gear contact ratio Γ and angular speed Ω_p, such that the system passes through multiple regimes on instability. The peak-to-peak transmission error is obtained for both the LTV and NLTV systems and their ratio is defined on a decibel scale as $L_\delta = 20 \log_{10}(\gamma)$ where $\gamma = \delta_{LTV}/\delta_{NLTV}$. This ratio is plotted in Figure 15, wherein a value of zero implies that the two analyses yield identical results. Conversely, a high value of the ratio indicates a smaller amplitude of response for the NLTV gear system. Over almost the entire range studied here, a positive or zero value of the ratio is obtained ($L_\delta \geqslant 0$). Since these results were obtained using numerical integration, we cannot find with absolute certainty all of the unstable zones. Nevertheless, in zones where this ratio is very large, we can infer that the LTV system yields an unstable response whereas the non-linearities could potentially provide a stable system.

Finally, this comparison is carried out for the whole range of frequencies, up to the natural frequency of the system (at $\Omega_p \approx 13{,}400$ rpm). Figure 16(a) shows the unstable zones for the LTV system as functions of the contact ratio and operating speed of the input gear. Here, super-harmonic as well as sub-harmonic resonances can be clearly seen as the shaded

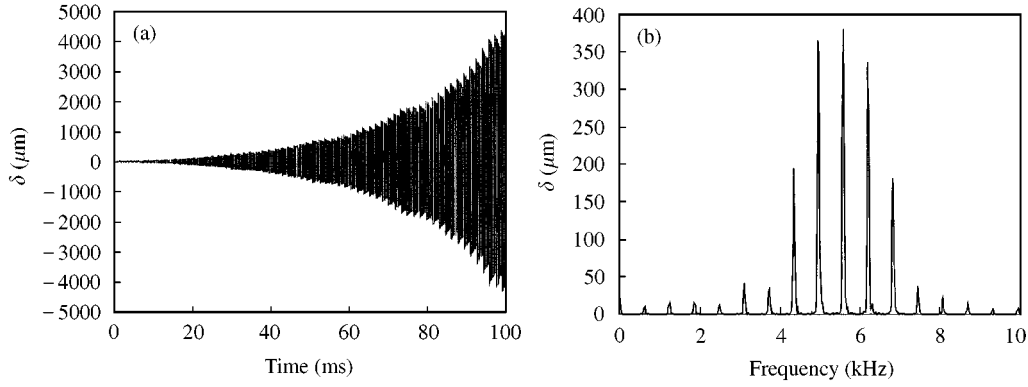

Figure 13. Dynamic response $\delta(t)$ with LTV analysis, near resonance conditions for $\zeta = 0{\cdot}001$, $\mu = 0{\cdot}1$, $\Omega = 1490$ rpm, $\Gamma = 1{\cdot}473$: (a) time-domain response; (b) frequency spectrum.

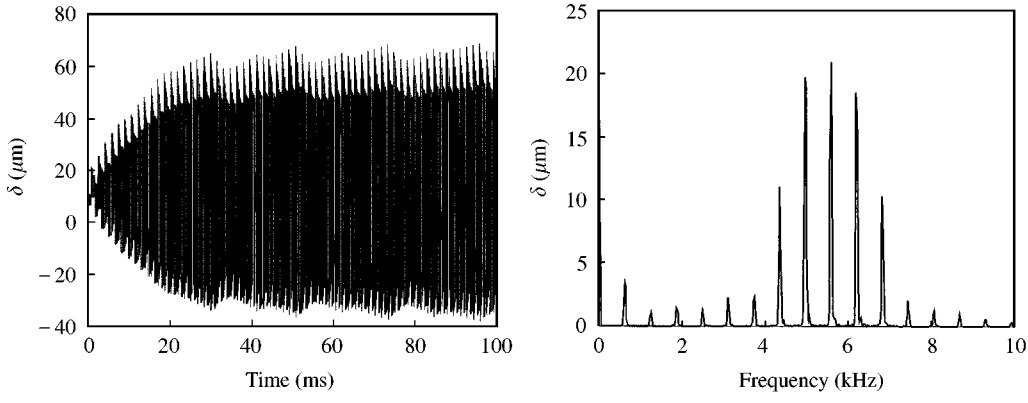

Figure 14. Dynamic response $\delta(t)$ with NLTV analysis, away from resonance conditions for $\zeta = 0{\cdot}001$, $\mu = 0{\cdot}1$, $\Omega = 1490$ rpm, $\Gamma = 1{\cdot}473$: (a) time-domain response; (b) frequency spectrum.

regions. The zones at sub-harmonics like $\omega_0 \approx 2\omega_n/3$ represent the period-doubling bifurcation whereas super-harmonics of ω_0 correspond to saddle-node bifurcation instabilities [11]. These unstable zones tilt towards the right because as Γ is increased, the time-averaged mesh stiffness goes up according to the relationship in equation (21) and hence the effective system natural frequency increases.

Figure 16(b) shows the contours of ratio of the magnitudes for LTV and NLTV cases similar to Figure 15. The maximum influence of friction non-linearities is observed at the primary resonance, i.e., for the zone with $\omega_0 = \omega_n$. In accordance with the limitations of numerical analyses, a value of γ needs to be determined as the threshold of stability. For the purpose of illustration, we have assumed that a value of $\gamma > 10^2$ distinguishes the stable and unstable regions. Therefore, the inner two contours represent the zones where a stable response has been achieved due to friction non-linearity. It is also clear from the figure that this is true both for the saddle-node bifurcation as well as the period-doubling instabilities. Thus, this analysis establishes some essential differences in the dynamic characteristics of sliding friction under LTV or NLTV considerations. It can be concluded that these differences are significant only near resonant conditions of the gear mesh. Consequently, sliding friction at the gear teeth, just like the inherent damping in the system, could provide

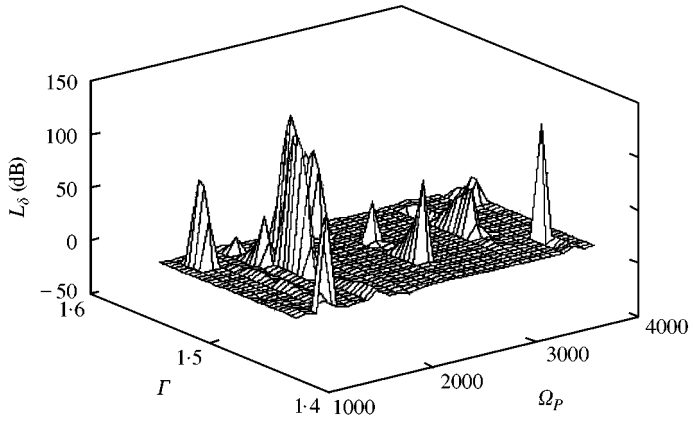

Figure 15. Plot of ratio L_δ for the dynamic transmission error using LTV and NLTV analyses.

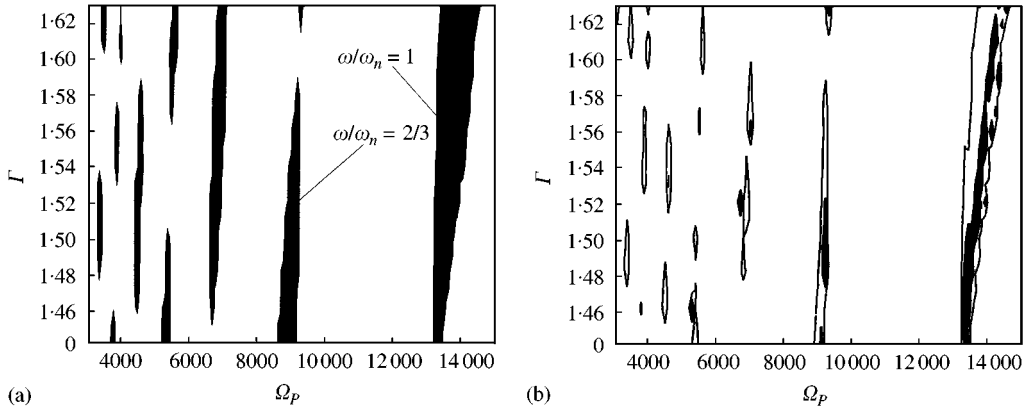

Figure 16. Stability plots over a wider frequency range, up to the natural frequency of the system. (a) contours of constant magnitude for LTV model showing unstable zones; (b) ratio γ of magnitude of δ between LTV and NLTV models. □, $\gamma = 3$; ■, $\gamma = 100$; ■, $\gamma = 100,000$.

one of the justifications for the absence of instabilities in most practical gearboxes, even though many of the failures are still ill-understood.

8. CONCLUSION

In this article, a new gear dynamic model is proposed which incorporates non-linearities induced by sliding friction. This model is compared with a linear time-varying system formulation and their salient dynamic characteristics are discussed. For the analysis of an LTV system, a multiterm harmonic balance scheme is developed with friction acting as an external excitation. This method is applied to analyze the influence of individual parameters as well as their dynamic interactions. Sub-harmonic terms are included in the solution and using these, the period-doubling instabilities are predicted in the system.

When the NLTV system is modelled using the HBM, the nature of sliding non-linearity leads to an extraordinarily large number of intractable equations and non-linear terms, and

hence numerical simulations are applied for these. The influence of sliding friction on the spectral composition of the dynamic response is studied. Both the tribological parameters and the kinematic phasing between the pitch point and the tooth contact transition points dictate the overall effect of sliding friction. Finally, the vibration damping characteristics of friction are investigated, which show that friction is able to reduce the large oscillations at certain resonant conditions. Thus, when compared with an LTV system, the regimes of instability shrink for a non-linear system. However, for non-resonant conditions, both LTV and NLTV systems yield identical results.

Many aspects of this study have potential for further research. A higher degree of freedom model could conceivably bring out a more pronounced effect of friction, especially when the system includes the translational dynamics in the sliding direction. It will also be of interest to incorporate the backlash non-linearity and examine the influence of loss of contact on the sliding characteristics. Although this article brings out the issue of stability, a detailed analysis of the types of stabilities and their individual relationship with friction terms should give a deeper insight into gear dynamics. More general cyclic variations of mesh stiffness can be considered to validate the model. Finally, it would be very desirable to design precisely controlled experiments that can aid in identifying the phenomenon of friction as well as the dynamic instabilities.

REFERENCES

1. K. F. MARTIN 1980 *Transactions of the American Society of Mechanical Engineers Paper no.* 80-C2/DET-16. The efficiency of involute spur gears.
2. P. VELEX and V. CAHOUET 2000 *Proceedings of the* 2000 *ASME Design Engineering Technical Conferences* DETC2000/PTG-14430, 1–10, Baltimore, U.S.A. Experimental and numerical investigations on the influence of tooth friction in spur and helical gear dynamics.
3. J. BORNER and D. R. HOUSER 1996 *Society of Automotive Engineers Technical Paper Series* 961816, 1–8. Friction and bending moments as gear noise excitations.
4. H. IIDA, A. TAMURA and Y. YAMADA 1985 *Bulletin of the Japanese Society of Mechanical Engineers* **28**, 1512–1519. Vibrational characteristics of friction between gear teeth.
5. E. RADZIMOVSKY and A. MIRAREFI 1974 *Journal of Engineering for Industry*, *Transactions of the American Society of Mechanical Engineers Paper no.* 74-DET-86, 1–7. Dynammic behavior of gear systems and variation of coefficient of friction and efficiency during the engagement cycle.
6. D. HOCHMANN 1997 *Ph.D. Dissertation*, *The Ohio State University*, *Columbus*, *OH*. Friction force excitations in spur and helical involute parallel axis gearing.
7. M. VAISHYA and R. SINGH 2001 *Journal of Sound and Vibration* **243**, 525–545. Analysis of periodically varying gear mesh systems with Coulomb friction using Floquet theory.
8. G. W. BLANKENSHIP and R. SINGH 1995 *Journal of Sound and Vibration* **179**, 13–36. Analytical solution for modulation sidebands associated with a class of mechanical oscillators.
9. H. N. OZGUVEN and D. R. HOUSER 1988 *Journal of Sound and Vibration* **121**, 383–411. Mathematical models used in gear dynamics—a review.
10. A. KAHRAMAN and R. SINGH 1990 *Journal of Sound and Vibration* **142**, 49–75. Non-linear dynamics of a spur gear pair.
11. C. PADMANABHAN and R. SINGH 1996 *Journal of Acoustical Society of America* **99**, 324–334. Analysis of periodically forced nonlinear Hill's oscillator with application to a geared system.
12. H. N. OZGUVEN 1991 *Journal of Sound and Vibration* **145**, 239–260. A non-linear mathematical model for dynamic analysis of spur gears including shaft and bearing dynamics.
13. T. IWATSUBO, S. ARII and R. KAWAI 1984 *Proceedings of the Third International Conference on Vibrations in Rotating Machinery*, *Institution of Mechanical Engineers*, 59–66. The coupled lateral torsional vibration of a geared rotor system.
14. A. KAHRAMAN and R. SINGH 1991 *Journal of Sound and Vibration* **146**, 135–156. Interactions between time-varying mesh stiffness and clearance non-linearities in a geared system.

15. S. OH, K. GROSH and J. R. BARBER 1998 *Proceedings of the National Conference on Noise Control Engineering, Institute of Noise Control Engineering*, 145–150. Dynamic behavior of interacting spur gears: energy conservation.
16. N. HINRICHS, M. OESTREICH and K. POPP 1998 *Journal of Sound and Vibration* **216**, 435–459. On the modeling of friction oscillators.
17. T. F. CONRY and A. SEIREG 1973 *Journal of Engineering for Industry, Transactions of the American Society of Mechanical Engineers* **95**, 1115–1122. A mathematical programming technique for the evaluation of load distribution and optimal modifications for gear systems.
18. B. W. KELLEY and A. J. LEMANSKI 1967 *Proceedings of Institution of Mechanical Engineers* **182**, 173–184. Lubrication of involute gearing.
19. M. VAISHYA and D. R. HOUSER 2000 *Proceedings of the* 2000 *ASME Design Engineering Technical Conferences* DETC2000/PTG-14431, 1–10. Modeling and analysis of sliding friction in gear dynamics.
20. M. BENTON and A. SEIREG 1978 *Journal of Mechanical Design, Transactions of the American Society of Mechanical Engineers* **100**, 26–32. Simulation of resonances and instability conditions in pinion-gear systems.
21. E. A. BARBASHIN 1970 *Introduction to the Theory of Stability*. Netherlands: Wolters-Noordhoff.
22. A. KAHRAMAN and G. W. BLANKENSHIP 1996 *Journal of Sound and Vibration* **194**, 317–336. Interactions between commensurate parametric and forcing excitations in a system with clearance.
23. F. OBERHETTINGER 1973 *Fourier Expansions A Collection of Formulas*. New York: Academic Press Inc.

APPENDIX A: NOMENCLATURE

a, b	Fourier coefficients for harmonic response
c, d	Fourier coefficients for sub-harmonic response
c	damping coefficient
F	force
f_0	gear meshing frequency
J	moment of inertia
K	matrix with stiffness and damping terms
k	mesh stiffness
L_c	length of line of contact
L_δ	ratio of dynamic response using LTV and NLTV analyses
N	normal load
n	number of harmonic terms
R	base circle radius
R_q	Compound surface roughness of mating parts
T	torque
t	time instant
V	velocity
V_t	total rolling velocity
V_0	reference velocity for non-dimensionalization
α	gear roll angle
δ	dynamic transmission error
ε	unloaded static transmission error
Γ	profile contact ratio of gears
γ	ratio of peak-to-peak transmission error in LTV and NLTV systems
η	axis along off-line of action
η_0	dynamic viscosity of lubricant
μ_0	material coefficient of friction
μ	instantaneous coefficient of friction
Π	number of teeth on the gears
θ	angle of rotation of gear or pinion
ρ	radius of curvature of contacting surface
Ω	mean angular speed
ω	excitation frequency
ξ	location on line of contact
ζ	damping ratio

Subscripts

1, 2	number of tooth in contact
a, *b*, *c*	time zone in gear mesh cycle
f	friction
h, *u*	harmonic and sub-harmonic respectively
i	index of particular tooth in contact
m	one mesh cycle
p, *g*	pinion and gear respectively
s	sliding

Abbreviations

LTV	linear time varying
NLTV	non-linear time varying
HBM	harmonic balance method